Journal of Materials Chemistry B

PAPER

View Article Online
View Journal | View Issue

Cite this: J. Mater. Chem. B, 2014, 2, 7725

Coacervate-directed synthesis of $CaCO_3$ microcarriers for pH-responsive delivery of biomolecules†

V. Lauth, M. Maas* and K. Rezwan

Received 22nd July 2014
Accepted 16th September 2014

DOI: 10.1039/c4tb01213e

www.rsc.org/MaterialsB

We report the synthesis of pH-responsive microcarriers *via* the combination of complex coacervation and mineralization of calcium carbonate ($CaCO_3$). Positively and negatively charged proteins (bovine serum albumin (BSA) and lysozyme (LSZ)) form electrostatic complexes with poly(acrylic acid) sodium salt (PAANa) and calcium ions in an aqueous solution, leading to the formation of spherical coacervate droplets. By the addition of sodium carbonate, the protein-loaded droplets are mineralized into stable $CaCO_3$ microcarriers. Since this inorganic material exhibits high solubility in acids, the release of protein from the carriers can be controlled *via* the pH of the environment. The process results in the successful generation of bulk amounts of monodisperse and colloidally stable microspheres with diameters as small as 300 nm. As the entire synthesis takes place under aqueous conditions, coacervate-directed encapsulation is suitable for sensitive active agents. Accordingly, the method presents a promising approach to synthesize pH-responsive microcarriers for drug delivery applications.

Introduction

Nanocarriers have established their place in biomedical applications as imaging and delivery vehicles.[1] Recently, several types of nano-based carriers are entering clinical trials.[2] However, due to restrictions on both ligand recognition and enhanced permeability and retention (EPR) effect, as well as the formation of complex nanoparticle coronas, nano-sized drug carriers still face critical barriers for the translation into clinics.[3,4] In order to enhance the bioavailability of drugs at the disease site, it is highly desirable to include stimuli responsive properties in the carriers.[1] The ability to trigger the release of active agents in response to endogenous changes can be largely exploited for the treatment of neoplastic diseases.[4] In this context, we designed a bio-inspired strategy for synthesizing pH-responsive microcarriers based on the combination of two well-studied approaches: complex coacervation and mineralization of calcium carbonate.

Besides lipids, most drug nanocarriers are based on polymeric materials,[2] due to their diversity, flexibility in synthesis methods and easy functionalization.[5] Amongst the various approaches for encapsulating active agents, coacervation has been used successfully for a long time, starting with the first description of the phenomenon by Bungenberg de Jong in 1929.[6] Two main types of coacervation have been described and differ by the phase separation mechanism. In simple coacervation, the mechanism involves partial desolvation or dehydration of macromolecules.[5,7] Complex coacervation, on the other hand, is induced by the electrostatic interaction and comprises two or more oppositely charged colloids. Both techniques are widely used in the food industry *e.g.* in order to retard the oxidation of fish oil,[8] or in cosmetics to encapsulate antioxidant oils.[9] Recent research reported the use of complex coacervation to encapsulate and deliver growth factors,[10] genes[11,12] as well as proteins.[13] Furthermore, coacervates are currently being investigated for their role in protocell formation and as models of protocell assembly.[14] Several advantages arise from the coacervation method, for example, good encapsulation efficiencies,[13] the ability of co-encapsulation and the conjugation of ligands for targeting approaches.[11] The major drawback of this approach is the high instability of the complexes which might necessitate the use of potentially toxic stylizers[15] or cross-linkers.[16] Moreover, in order to introduce pH-responsive behavior to the coacervates, additional molecules might have to be added. For instance, pyranine-3 was used to produce pH sensitive microcapsules based on the self-assembly of nanoparticles on the surface of coacervate droplets.[17]

By mineralizing the coacervates with inorganic materials that have high solubility in acids while being stable at neutral and basic pHs, it is possible to stabilize the coacervates, as well as to introduce pH-responsive behavior. One material that suits this purpose is calcium carbonate ($CaCO_3$). It has long been suggested as a drug carrier due to its biocompatibility and biodegradability, low cell cytotoxicity and cost-effectiveness.[18] One common procedure for encapsulation and sustained

Advanced Ceramics, University of Bremen, Am Biologischen Garten 2, 28359 Bremen, Germany. E-mail: michael.maas@uni-bremen.de

† Electronic supplementary information (ESI) available. See DOI: 10.1039/c4tb01213e

release of biomolecules with $CaCO_3$ is the direct crystallization method.[19–21] The incorporation of proteins is achieved by physical adsorption onto the synthesized crystals.[19–21] The main characteristics of the produced carriers are their large particle size (1–5 μm), crystalline polymorphism and highly porous structure.[21] Some disadvantages arise from this technique, such as the crystalline structure, which is subject to recrystallization in water which might lead to changes in shape or polymorphism.[20] Calcium carbonate nanoparticles produced by this technique are often used as templates to synthesize layer-by-layer polymer microcapsules.[19]

Another method for the synthesis of $CaCO_3$ particles that are loaded with active agents is co-precipitation. Here, the precipitation of calcium carbonate is initiated in a solution that already contains the molecules to be encapsulated, *e.g.* anti-inflammatory drugs,[22] hormones,[23] proteins,[20] genes[24–26] and antigens.[27] The morphology of products prepared *via* coprecipitation is rather heterogeneous, featuring macrosized plates or rods[22] as well as nanosized particles.[23] Emulsion-based co-precipitation has also been used to encapsulate pesticides,[28] genes[29] and growth factors.[30] In this approach, emulsions containing calcium chloride, surfactants and biomolecules are produced and the precipitation of nanocarriers is promoted by the addition of sodium carbonate. High encapsulation efficiencies can be obtained by the co-precipitation method.[24]

In the aforementioned approaches, the lack of control of morphology and polymorphism of the carriers is the main drawback. Polymers,[31] polysaccharides[32,33] or even proteins[34] can be used to modify the crystallization pathway of calcium carbonate and allow the control of the morphology and the stabilization of specific polymorphisms. This method is known as polymer-controlled mineralization and results in either nanoparticles[32] or highly porous, micron-sized particles.[34] The wide variety of polymers and polyelectrolytes that can be used enables the synthesis of pH and temperature responsive carriers.[35,36] The incorporation of anti-cancer drugs[35,37] and proteins[33] can be either performed by physical adsorption after mineralization of the carriers[34] or by co-precipitation.[32]

In our work, we demonstrate a bio-inspired strategy for synthesizing pH-responsive submicron-sized carriers based on the combination of complex coacervation and mineralization. Our group first modified a polymer-controlled approach proposed by Huang *et al.*[38] in order to produce micropatterned parts[39] and to encapsulate model proteins. The coacervate-directed method (Scheme 1) starts with complex coacervation between negatively or positively charged biomolecules and poly(acrylic acid) sodium salt (PAANa). The polymer is used as an additive to modify mineralization, to stabilize amorphous calcium carbonate (ACC) and to incorporate the proteins into the coacervate droplets. In order to stop complexation and to stabilize the loaded droplets, sodium carbonate is added to the solution leading to the mineralization of the complex. Since the entire encapsulation process takes place in aqueous solutions, at room temperature and mild pH, the main benefits are the preservation of the bioactivity of the encapsulated biomolecules as well as the ability to easily scale up the system. Therefore, coacervate-directed microcarriers are highly promising for potential use in gene, drug, protein and growth factor delivery.

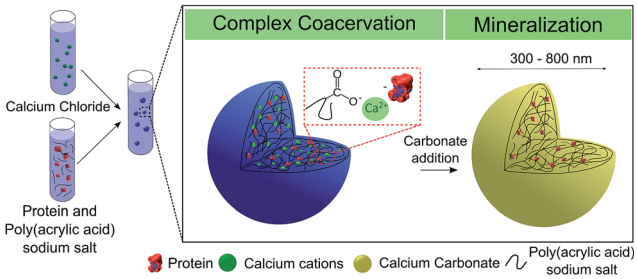

Scheme 1 Schematic synthesis approach of coacervate-directed $CaCO_3$ microcarriers: complex coacervation between PAANa and the proteins in aqueous solution generates loaded-coacervate droplets which are subsequently mineralized by the addition of sodium carbonate.

Experimental

Materials

Calcium chloride ($CaCl_2$, purity ≥ 96%), sodium carbonate (Na_2CO_3, purity ≥ 99.5%), poly(acrylic acid) sodium salt (PAANa, M_w = 8000 g mol^{-1}, 45 wt% in water), bovine serum albumin (BSA, lyophilized powder, purity ≥ 96%) and lysozyme (LSZ, lyophilized powder, purity ≥ 90%) were purchased from Sigma-Aldrich and used without any further purification. The experiments were performed using double deionized water with a conductivity of 0.04 μS cm^{-1} from Synergy (Millipore, Darmstadt, Germany).

Synthesis of $CaCO_3$ and incorporation of proteins

Briefly, 40 mL aqueous solution of PAANa and $CaCl_2$ was prepared resulting in a final concentration of the polyelectrolyte ranging from 700 to 1900 μg mL^{-1} with a fixed calcium concentration of 12 mM. The complexation between Ca^{2+} and PAANa takes place immediately after mixing and leads to the phase-separation of liquid-like complex coacervates. These droplets are highly hydrated Ca^{2+}/PAA complexes dispersed in the polymer-poor aqueous solution. After a specific period of time, the complexation time, 12 mM Na_2CO_3 was added. Since one of the main components of the coacervate droplets is calcium cations, the addition of carbonate mineralizes the complex. The samples were centrifuged (5000 rpm, 10 minutes) and the obtained precipitate was dried at room temperature for 2 days. The bulk amount of carriers produced per batch is dependent on the solution's volume which allows easy scale-up of the process.

In order to prepare protein-loaded carriers, the respective biomolecules were dispersed in the aqueous solution prior to the addition of PAANa and $CaCl_2$. The final concentration of proteins ranged from 0.2 to 0.3 mg mL^{-1} and all other parameters were maintained the same.

Release behavior of proteins

The obtained protein-loaded $CaCO_3$ microcarriers were dried in air, weighed (about 20–30 mg per batch) and resuspended in 0.54 mL of acetic acid (pH 4.8), PBS buffer (pH 6) or PBS buffer (pH 7.4). The samples were mildly shaken for 200 hours at room temperature. An aliquot of 350 μL was removed at each measurement time-point and replaced with an equal volume of the same buffer. The removed aliquot was centrifuged at 5000 rpm for 15 minutes and the protein concentration was determined by UV-Visible spectroscopy at 280 nm. The absorbance of polyacrylate was evaluated at this wavelength and is negligible. The biomolecule content and loading efficiencies are calculated as follows (eqn (1) and (2)):

$$\text{Biomolecule content } (\text{nM mg}^{-1}) = \frac{\text{quantified amount of biomolecules (nM)}}{\text{total weight of microcarriers (mg)}} \quad (1)$$

$$\text{Loading efficiency}(\%) = \frac{\text{quantified amount of biomolecules (nM)}}{\text{initial amount of biomolecules (nM)}} \times 100\% \quad (2)$$

Characterization of coacervate droplets and $CaCO_3$ microcarriers

Dynamic light scattering (DLS) as well as zeta-potential measurements were performed on a zetasizer device (Malvern, Nano ZSP). The morphology of the carriers was evaluated by scanning electron microscopy (Zeiss, SUPRA 40), with an acceleration voltage of 15 kV. X-ray diffraction (XRD) analysis was carried out using a JSO-Debyeflex 2002 device, with CuKα radiation ($k = 1.542$ A). The samples were ground to form a fine powder and scanned from 20° to 50°, 10 seconds per degree. UV-Vis spectroscopy was performed on a Multiskan G0 device (Thermo Scientific) at 280 nm.

Results

Influence of complexation time and protein incorporation on the coacervate droplet size

The electrostatic interaction of Ca^{2+} cations with PAANa induces the self-assembly of complex coacervate droplets. These are small complexes with an average size ranging from 200 to 400 nm formed by liquid–liquid phase separation from the initial solution. As mentioned above, this entropy-driven phenomenon is also known as complex coacervation,[40] although the term is largely missing in more recent literature, where it is sometimes replaced by purely descriptive terms.[41] The main characteristics of the coacervates are high instability (since it is a metastable phase) as well as liquid-like behavior. As a result of these characteristics, after nucleation, the coarsening of the droplets happens most likely through diffusion and accumulation of the polymer and Ca^{2+}.[42] Ostwald ripening does not seem to play a role as a growth mechanism since the polydispersity of the coacervates remains constant over time and the tail of the size distribution curve is located on the large-diameter side (ESI Fig. S1†).[43] Fig. 1 depicts the tendency of growth as a function of complexation time as well as the influence of the polyelectrolyte and proteins on the droplet size.

For native coacervates (Ca^{2+}/PAANa in the absence of proteins), the initial size is highly dependent on the PAANa concentration. By increasing the polymer concentration, the number of nucleation sites is increased along with a reduction in the particle size. Moreover, the droplets grow at different rates depending on the polymer concentration. For 700 μg mL^{-1} of PAANa, coacervates grow steadily within the 14 minute experiment, while for 1900 μg mL^{-1} this growth behavior is no longer noticeable. The growth process is related to the stability of the coacervates in solution. Since the coacervate droplets are electrostatically stabilized, droplets with higher net charges are less susceptible to aggregation and growth (ESI Fig. S2†).[44,45] Moreover, it is possible to tailor the size by controlling the polymer concentration; if the concentration is increased from 700 to 1900 μg mL^{-1}, the particle size decreases from 800 nm to 300 nm.

BSA-loaded coacervates were prepared with the final BSA concentration of 0.2 g L^{-1}. The incorporation of BSA slightly decreases the coacervate size compared to unloaded droplets. The rate at which the coacervates grow is not affected by the incorporation of BSA (Fig. 1).

When lysozyme is incorporated into the droplets, the coacervate size drastically changes (Fig. 1). The effect of LSZ on the coacervates is thought to be related to the formation of another complex coacervate, comprised of LSZ and PAANa. The electrostatic interaction of LSZ with PAANa is described in previous studies.[46,47] These complexes are larger than Ca^{2+}/PAANa, ranging from 800 nm to 1.2 μm, depending on the polymer concentration. This can be explained by the increased incorporation of LSZ due to stronger complexation compared to BSA. Furthermore, diffusion-controlled transport is still the predominant growth mechanism and reveals the metastability of the complex.

Characterization of mineralized microcarriers

As seen from the DLS results (Fig. 1), the size of coacervate droplets is highly dependent on the complexation time (tendency to grow over time as a result of the liquid-like behavior) and the polymer concentration. Based on this, it is possible to tailor the size of the final microcarriers by tweaking these two parameters. Since small carriers are desired for drug delivery applications, the complexation time was set to 1 minute and sodium carbonate was added to the solution in order to mineralize the microcarriers. Fig. 2 summarizes the final size of native, BSA and LSZ-loaded microcarriers measured by DLS. For native and BSA-loaded ones, increasing the polymer concentration yields smaller carriers. However, for LSZ-loaded carriers this tendency is no longer observed due to the formation of larger LSZ/PAANa coacervates.

The morphology of carriers has been shown to affect the cellular uptake of nanoparticles[48] and therefore this facet was assessed by SEM (Fig. 3). The incorporation of both negatively and positively charged molecules does not seem to influence

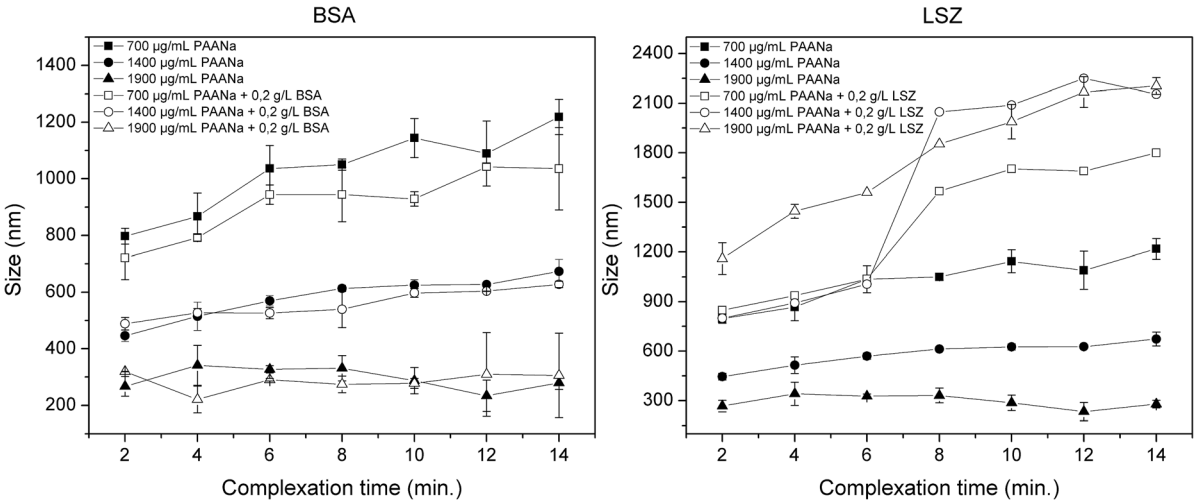

Fig. 1 Dynamic Light Scattering (DLS) overview of the mineralized microcarrier size as a function of PAANa concentration: native, BSA and LSZ-loaded microcarriers. $[Ca^{2+}] = [CO_3^{2-}]$ was kept constant at 12 mM. Each value is represented as a mean ± standard deviation of 3 samples.

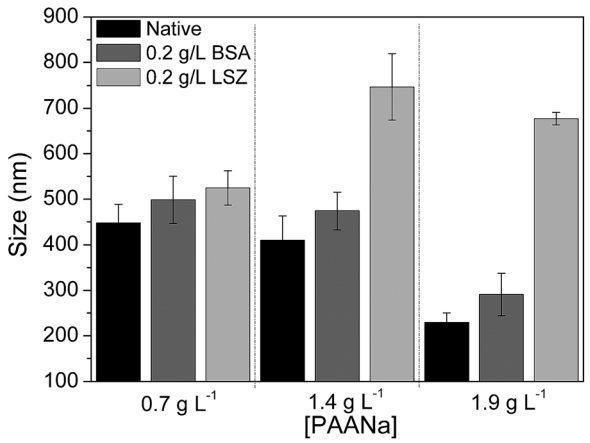

Fig. 2 Dynamic Light Scattering (DLS) overview of the mineralized microcarrier size as a function of PAANa concentration: native, BSA and LSZ-loaded microcarriers. $[Ca^{2+}] = [CO_3^{2-}]$ was kept constant at 12 mM. The complexation time was set to 1 minute. Each value is represented as a mean ± standard deviation of 3 samples.

the spherical geometry of the mineralized microcarriers. In the case of LSZ loading, smaller particles of about 20 nm can be observed to be adsorbed to the bigger particles. Since mineralization takes place under high supersaturation conditions, these small, unstable particles are formed and adsorbed at the surface of the mineralized coacervate droplets.[39] For all samples, the size of the mineralized microcarriers is consistent with the DLS data. In some of the samples, formation of open capsules could be observed. Note, however, that the intact carriers are not hollow, as was confirmed by STEM analysis (ESI Fig. S3†).

Zeta potential measurements can be used to assess the adsorption behavior of the molecules onto the surface of the particles. For carriers loaded with LSZ, by increasing the LSZ concentration from 0 to 0.5 g L^{-1}, the zeta potential changes from −35 to −26 mV (Table 1). Most likely, positively charged LSZ is adsorbed on the surface of negatively charged carriers. The zeta potential measured for BSA remains constant at about −35 mV, which means that absorption does not seem to take place, mainly due to electrostatic repulsion between negatively charged BSA and $CaCO_3$.

The amorphous polymorphism of the samples was verified by XRD analysis (ESI Fig. S4†). Hydrophilic polymers are well known to stabilize the amorphous phase as well as to alter the morphology of the final product.[31] The various effects of LSZ[49] and BSA[34] on the stabilization of polymorphism and morphology of $CaCO_3$ are also reported in the literature.

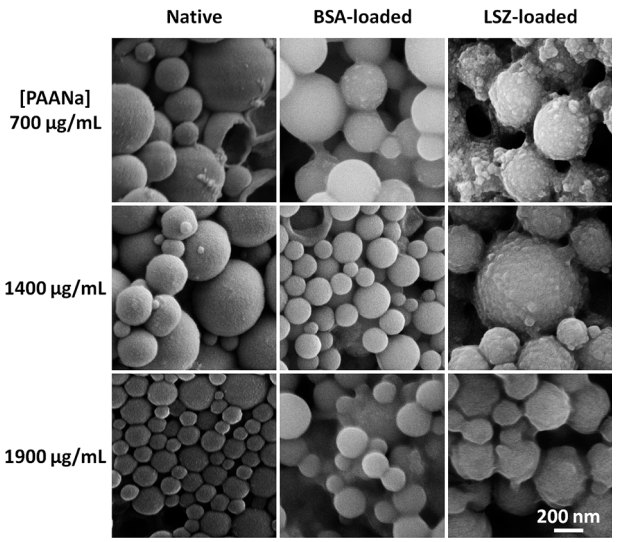

Fig. 3 SEM micrographs of native, BSA and LSZ-loaded microcarriers as a function of PAANa concentration (700, 1400 and 1900 µg mL^{-1}). $[Ca^{2+}] = [CO_3^{2-}]$ was kept constant at 12 mM. The complexation time was set to 1 minute.

Table 1 Zeta potential (mV) of microcarriers as a function of protein concentration. Measurements were performed at pH 9 and 1400 g L^{-1} of PAANa. Each value is represented as a mean ± standard deviation of 3 samples

Protein concentration	0 g L^{-1}	0.2 g L^{-1}	0.5 g L^{-1}
BSA	−35.68 ± 2.41	−31.14 ± 4.50	−37.09 ± 6.92
LSZ	−35.68 ± 2.41	−28.24 ± 3.21	−26.14 ± 4.01

Incorporation of proteins

The yield of carriers, loading efficiency and biomolecule content are detailed in Fig. 4. For all experiments, the yield of carriers is around 20 mg, even with the incorporation of BSA or LSZ. Moreover, according to the UV measurements, 0.23 nM of BSA were encapsulated per milligram of $CaCO_3$ carriers, resulting in an efficiency of about 0.2%. The scarce encapsulation of BSA was probably caused by the electrostatic repulsion of PAANa and BSA, since both of them are negatively charged at a synthesis pH of 7. However, the LSZ experiment showed that 7–8 nM of LSZ were encapsulated per milligram of $CaCO_3$ carriers, which equals an efficiency of 17–33%. Most likely, the electrostatic attraction between PAANa and LSZ is responsible for the better efficiency.

Release of proteins from microcarriers

The amounts of proteins released from the carriers are cumulatively plotted in Fig. 5. The release profile is highly pH dependent, which suggests that the main mechanism of release is the dissolution of the carriers.

At neutral pH, the complete BSA content is released within 50 hours (Fig. 5). If the experiments are performed at pH 4.8, the same amount of protein is released within a tenth of that time, 5 hours. Experiments that were performed at pH 6 showed a similar release behavior to that at pH 7. In general, BSA-loaded carriers show a rapid release curve at all evaluated pHs when compared to LSZ. Moreover, the release of BSA was completed before full dissociation of the carriers, which leads to two

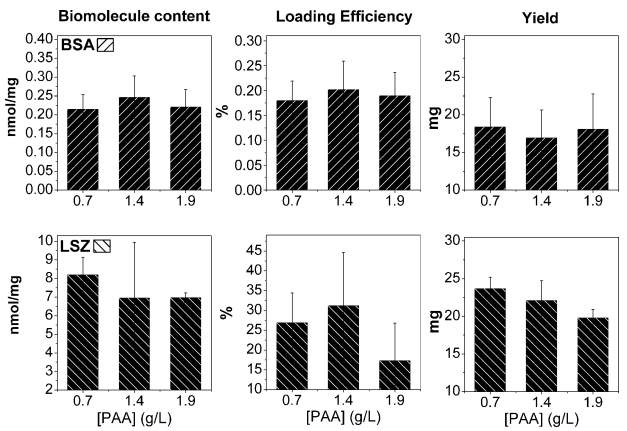

Fig. 4 Yield of carriers, loading efficiency and biomolecule content for BSA and LSZ loaded carriers. Each value is represented as a mean ± standard deviation of 3 samples.

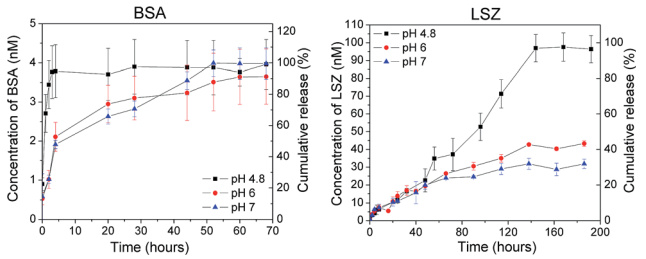

Fig. 5 Release profiles of BSA and LSZ from microcarriers in acetic acid pH 4.8, PBS buffer pH 6 and 7.4. Each value is represented as a mean ± standard deviation of 3 samples.

conclusions, (a) BSA is physically adsorbed to the surface of the carriers and therefore the release is desorption-dependent or (b) the molecules are encapsulated close to the surface of the carrier, which leads to complete release without full dissociation of the particles. By analysing the zeta potential measurements, the first hypothesis is unlikely, since the zeta potential remains constant with varying BSA concentrations (Table 1).

Regarding LSZ, the release profile shows sustained release over time with a notable absence of a burst release. At pH 4.8, LSZ was fully released within 140 hours while at neutral pH the release reaches a plateau after 80 hours of about 30% of release. At pH 6, the release behavior was slightly faster than at pH 7. Both at pH 6 and 7.4, the release was slow and incomplete. The cationic nature of this protein ($pK_a = 11.35$) gives rise to electrostatic interactions with the negatively charged carriers preventing complete release. Another possible explanation lies in the electrostatic nature of the complex LSZ/PAANa. If the pH is decreased, the net charge of PAANa is reduced which weakens the complex and allows a complete release.

Burst release of biomolecules from inorganic porous carriers has been reported elsewhere.[50] In the case of calcium carbonate, it is mostly associated with the polymorph stability.[22] Since the carriers are amorphous, the most unstable polymorph of $CaCO_3$, burst release could be expected. However, due to the introduction of PAANa, which stabilizes the carrier, the initial burst release can be avoided.

Proposed mechanism for protein encapsulation and release behavior

The incorporation of proteins is based on the electrostatic interaction between PAANa and the respective molecule. In the case of BSA (Scheme 2a), calcium plays two roles: (1) it favors the formation of complex coacervate droplets comprised of highly hydrated Ca^{2+}/PAANa and (2) it binds to both the carboxylate groups and the negative sites of BSA, forming the complex PAANa/Ca^{2+}/BSA,[51] which is responsible for encapsulation. The Ca^{2+}-mediated complex is only moderately effective in incorporating BSA (0.21 nM per mg of sample) and therefore results in low encapsulation capacities (0.02%).

By contrast, in the case of LSZ, two complex coacervation phenomena take place simultaneously: (1) complex coacervation of Ca^{2+}/PAANa and (2) complex coacervation of LSZ/PAANa, which is responsible for encapsulation (Scheme 2b). The

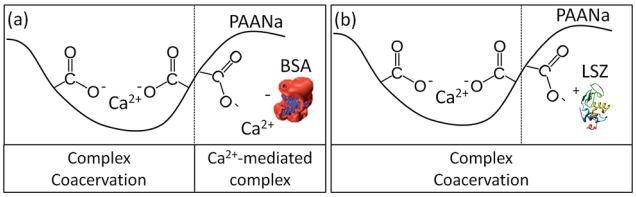

Scheme 2 Proposed mechanism for encapsulation of (a) BSA and (b) LSZ into the coacervate droplets.

competitive effect between the complexes leads to the formation of larger carriers with larger size and broader size distribution. Due to strong electrostatic interactions between the polyelectrolyte and protein, higher encapsulation efficiencies ($\approx$25%) are obtained.

After formation of the coacervates, Na_2CO_3 is added in order to stabilize the droplets by forming fully mineralized amorphous $CaCO_3$ particles. This material exhibits a good solubility in acid environments allowing the triggered release of proteins by adjusting the pH of the solution (Fig. 5). BSA molecules are encapsulated close to the surface of the carrier and are rapidly and completely released after 50 hours. Confocal imaging is usually used to confirm the encapsulation and distribution of stained-proteins within microcarriers. However, due to the nanoscopic nature of the carriers, such an experiment will not bring relevant information with regard to protein distribution within the carriers. The release of LSZ is slow and incomplete due to the electrostatic interaction between the protein and the negatively charged carriers.

Conclusions

In summary, the coacervate-directed mineralization approach allows the synthesis of pH-responsive carriers loaded with both negatively charged BSA and positively charged LSZ. The synthesis starts by complexating PAANa and the respective protein within coacervate droplets, whose sizes can be tailored by the polymer concentration and the complexation time. In order to stabilize the protein-loaded coacervate droplets and functionalize them with pH-responsive behavior, the complexes were mineralized *via* the addition of carbonate. The fully mineralized $CaCO_3$ microspheres had a diameter between 300 and 800 nm, exhibited spherical morphology and were loaded with BSA and LSZ at 0.2 nM and 8 nM per milligram of $CaCO_3$, respectively. As expected, the release behavior of the proteins was triggered by changes in pH. BSA molecules were rapidly and completely released after 50 hours while the release of LSZ is slow and incomplete due to the electrostatic interaction between the protein and the negatively charged carriers. Based on these features, we think that the coacervate-directed method presents a cost-effective, easy to scale-up way to synthesize tailorable submicron-sized, pH-responsive $CaCO_3$ carriers, which can be potentially used in gene, drug and growth factor delivery.

References

1 S. Ganta, H. Devalapally, A. Shahiwala and M. Amiji, *J. Controlled Release*, 2008, **126**, 187–204.
2 D. Peer, J. M. Karp, S. Hong, O. C. Farokhzad, R. Margalit and R. Langer, *Nat. Nanotechnol.*, 2007, **2**, 751–760.
3 M. P. Monopoli, C. Åberg, A. Salvati and K. A. Dawson, *Nat. Nanotechnol.*, 2012, **7**, 779–786.
4 S. Mura, J. Nicolas and P. Couvreur, *Nat. Mater.*, 2013, **12**, 991–1003.
5 J. Nicolas, S. Mura, D. Brambilla, N. Mackiewicz and D. M. Haddleton, *Chem. Soc. Rev.*, 2013, **42**, 1147–1235.
6 B. de Jong and H. R. Kruypz, *Proc. K. Ned. Akad. Wet.*, 1929, **32**, 849–856.
7 R. Arshady, *Polym. Eng. Sci.*, 1990, **30**, 905–914.
8 B. Wang, B. Adhikari and C. J. Barrow, *Food Chem.*, 2014, **158**, 358–365.
9 I. M. Martins, S. N. Rodrigues and F. Barreiro, *J. Microencapsulation*, 2009, **26**, 667–675.
10 H. K. Awada, N. R. Johnson and Y. Wang, *Macromol. Biosci.*, 2014, **14**, 679–686.
11 K. Leong, H.-Q. Mao, V. Truong-Le, K. Roy, S. Walsh and J. August, *J. Controlled Release*, 1998, **53**, 183–193.
12 Y. Yuan, J. Tan, Y. Wang, C. Qian and M. Zhang, *Acta Biochim. Biophys. Sin.*, 2009, **41**, 515–526.
13 N. Ray, T. Ambe and Y. Wang, *Acta Biomater.*, 2014, **10**, 40–46.
14 S. Mann, *Acc. Chem. Res.*, 2012, **45**, 2131–2141.
15 C. Sanchez and D. Renard, *Int. J. Pharm.*, 2002, **242**, 319–324.
16 C. L. Cooper, P. L. Dubin, A. B. Kayitmazer and S. Turksen, *Curr. Opin. Colloid Interface Sci.*, 2005, **10**, 52–78.
17 A. J. Amali, S. Singh, N. Rangaraj, D. Patra and R. K. Rana, *Chem. Commun.*, 2012, **48**, 856–858.
18 R. Kurapati and A. M. Raichur, *J. Mater. Chem. B*, 2013, **1**, 3175–3184.
19 D. V. Volodkin, N. I. Larionova and G. B. Sukhorukov, *Biomacromolecules*, 2004, **5**, 1962–1972.
20 A. I. Petrov, D. V. Volodkin and G. B. Sukhorukov, *Biotechnol. Prog.*, 2005, **21**, 918–925.
21 G. B. Sukhorukov, D. V. Volodkin, A. M. Günther, A. I. Petrov, D. B. Shenoy and H. Möhwald, *J. Mater. Chem.*, 2004, **14**, 2073–2081.
22 U. Maver, M. Bele and J. Jamnik, *Mater. Res.*, 2013, **48**, 137–145.
23 Y. Ueno, H. Futagawa, Y. Takagi, A. Ueno and Y. Mizushima, *J. Controlled Release*, 2005, **103**, 93–98.
24 C.-Q. Wang, J.-L. Wu, R.-X. Zhuo and S.-X. Cheng, *Mol. BioSyst.*, 2014, **10**, 672–678.
25 S. Chen, D. Zhao, F. Li, R.-X. Zhuo and S.-X. Cheng, *RSC Adv.*, 2012, **2**, 1820.
26 T. Borodina, E. Markvicheva, S. Kunizhev, H. Möhwald, G. B. Sukhorukov and O. Kreft, *Macromol. Rapid Commun.*, 2007, **28**, 1894–1899.
27 S. De Koker and B. De Geest, *Angew. Chem., Int. Ed.*, 2009, **48**, 8485–8489.

28 K. Qian, T. Shi, T. Tang, S. Zhang, X. Liu and Y. Cao, *Microchim. Acta*, 2010, **173**, 51–57.
29 M. Fujiwara, K. Shiokawa and K. Morigaki, *Chem. Eng. J.*, 2008, **137**, 14–22.
30 X. He, T. Liu, Y. Chen, D. Cheng and X. Li, *Cancer Gene Ther.*, 2008, **15**, 193–202.
31 H. Cölfen, *Top. Curr. Chem.*, 2007, **271**, 1–77.
32 D. Zhao, R.-X. Zhuo and S.-X. Cheng, *Mol. BioSyst.*, 2012, **8**, 753–759.
33 Z. Lu, J. Zhang, Y. Ma, S. Song and W. Gu, *Mater. Sci. Eng., C*, 2012, **32**, 1982–1987.
34 N. Qiu, H. Yin, B. Ji, N. Klauke, A. Glidle, Y. Zhang, H. Song, L. Cai, L. Ma, G. Wang, L. Chen and W. Wang, *Mater. Sci. Eng., C*, 2012, **32**, 2634–2640.
35 C. Du, J. Shi, J. Shi, L. Zhang and S. Cao, *Mater. Sci. Eng., C*, 2013, **33**, 3745–3752.
36 J. Shi, W. Qi, C. Du and S. Cao, *J. Appl. Polym. Sci.*, 2013, 577–584.
37 J. Shi, J. Shi, D. Feng, P. Yue and S. Cao, *Polym. Bull.*, 2014, **71**, 1857–1873.
38 S. Huang, K. Naka and Y. Chujo, *Langmuir*, 2007, **23**, 12086–12095.
39 P. Kaempfe, V. R. Lauth, T. Halfer, L. Treccani, M. Maas and K. Rezwan, *J. Am. Ceram. Soc.*, 2013, **96**, 736–742.
40 C. G. De Kruif, F. Weinbreck and R. De Vries, *Curr. Opin. Colloid Interface Sci.*, 2004, **9**, 340–349.
41 B. Cantaert, Y. Kim, H. Ludwig, F. Nudelman, N. A. J. M. Sommerdijk and F. C. Meldrum, *Adv. Funct. Mater.*, 2012, **22**, 907–915.
42 C. Sanchez, G. Mekhloufi and D. Renard, *J. Colloid Interface Sci.*, 2006, **299**, 867–873.
43 C. G. Granqvist and R. A. Buhrman, *J. Catal.*, 1976, **42**, 477–479.
44 V. S. Murthy, R. K. Rana and M. S. Wong, *J. Phys. Chem. B*, 2006, **110**, 25619–25627.
45 C. Sanchez, G. Mekhloufi, C. Schmitt, D. Renard, P. Robert, C. Lehr, A. Lamprecht and J. Hardy, *Langmuir*, 2002, **18**, 10323–10333.
46 D. Romanini, M. Braia, R. Giatte, W. Loh and G. Pic, *J. Chromatogr. B: Anal. Technol. Biomed. Life Sci.*, 2007, **857**, 25–31.
47 A. Ghimire, R. M. Kasi and C. V. Kumar, *J. Phys. Chem. B*, 2014, **118**, 5026–5033.
48 H. Herd, N. Daum, A. T. Jones, H. Huwer, H. Ghandehari and C. Lehr, *ACS Nano*, 2013, **7**, 1961–1973.
49 X. Wang, H. Sun, Y. Xia, C. Chen and H. Xu, *J. Colloid Interface Sci.*, 2009, **332**, 96–103.
50 C. Wang, C. He, Z. Tong, X. Liu, B. Ren and F. Zeng, *Int. J. Pharm.*, 2006, **308**, 160–167.
51 M. Karahan, Z. Mustafaeva and C. Ozeroğlu, *Protein J.*, 2010, **29**, 336–342.